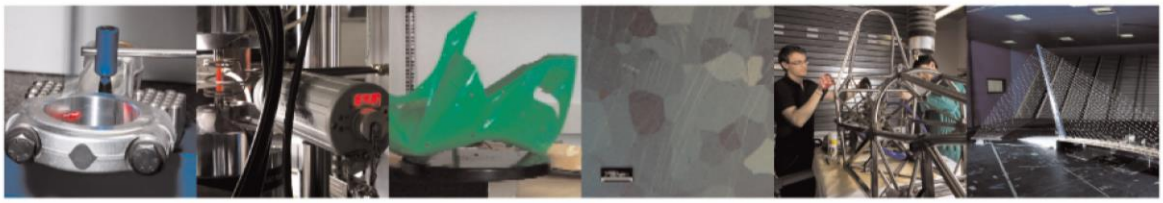

Surface finishing by laser re-melting applied to robotized laser metal deposition

Francesco Bruzzo, Guendalina Catalano, Ali Gökhan Demir, Barbara Previtali

This is a post-peer-review, pre-copyedit version of an article published in Optics and laser in engineering. The final authenticated version is available online at:
http://dx.doi.org/10.1016/j.optlaseng.2020.106391

DIPARTIMENTO DI MECCANICA ■ POLITECNICO DI MILANO
via G. La Masa, 1 ■ 20156 Milano ■ EMAIL (PEC): pecmecc@cert.polimi.it
http://www.mecc.polimi.it
Rev. 0

Surface finishing by laser re-melting applied to robotized laser metal deposition

Francesco Bruzzo, Guendalina Catalano, Ali Gökhan Demir*, Barbara Previtali
Department of Mechanical Engineering, Politecnico di Milano, Via La Masa 1, 20156 Milan, Italy
**Corresponding author: aligokhan.demir@polimi.it*

Surface finishing by laser re-melting applied to robotized laser metal deposition

Francesco Bruzzo, Guendalina Catalano, Ali Gökhan Demir*, Barbara Previtali
Department of Mechanical Engineering, Politecnico di Milano, Via La Masa 1, 20156 Milan, Italy
**Corresponding author: aligokhan.demir@polimi.it*

Abstract

Low surface quality of as-deposited laser metal deposition (LMD) parts is one of the main drawbacks of this additive manufacturing technology that prevents direct use without the implementation of costly and time consuming post-processes. An in-process surface finishing operation without the need of auxiliary equipment is highly appealing to overcome such issues. For this reason, laser re-melting performed with the same laser equipment used for the deposition process is a promising technology capable of redistributing the deposited material onto a smoother surface. Combined with a robotic manipulation system used for both the LMD and laser re-melting phases, complex geometries can potentially be produced in near net-shape conditions. An important issue concerning development of this process development regards the use of standardized roughness and waviness parameters, which can fail to address the texture specific to the LMD process. Indeed, the laser re-melting process can produce new texture formation under non-optimal conditions. Hence, an analysis of the surface topography in the frequency domain along with the standard surface roughness and waviness parameters would be more appropriate. In this work, laser re-melting is applied to AISI 316L thin walled structures right after the deposition process. An experimental campaign aimed at finding the process parameters and re-melting strategy capable of improving the surface quality was carried out. Areal surface profile measurements were used for characterizing the effect of the process parameters. The surface power spectrum on the S-F surface was calculated to point out the presence of periodical components in the surface structure and a transfer function calculation was performed to define the surface quality improvement in the frequency domain compared to the LMD as-deposited surface. The acquired surface areal data was assessed at two different frequency regions corresponding to the S-L and L-F surfaces. The arithmetic average of the filtered surface areal data was used to calculate $S_{a,SF}$ and $S_{a,LF}$ analogously to the roughness and waviness parameters of linear measurements respectively. Results showed, in the optimized conditions, a reduction of up to 80% in the roughness related frequency range. On the other hand, the waviness parameter is reduced up to 58% due to the low effectiveness of laser re-melting in reducing the amplitude of the lowest frequency components. The overall improvement in terms of process capability was evaluated as mean ± 3 times the sample standard deviation values (μ±3σ). The average surface roughness $S_{a,SF}$ could be reduced from 10.35±0.42 μm to 1.92±0.11 μm and average surface waviness $S_{a,LF}$ from 9.57±0.48 μm to 4.04±0.20 μm.

Keywords: Directed energy deposition; hybrid manufacturing; laser polishing; robotic manipulation.

1. INTRODUCTION

Laser metal deposition (LMD) is an additive manufacturing process employable for producing medium to large components with bulky and thin-walled features. It is especially suited to producing axial-symmetric parts developing around a machine axis. Moreover, LMD is can be used both to build new parts or to add features and to repair already existing components [1,2]. As a matter of fact, LMD has a higher potential of geometric flexibility and accessibility when integrated with robotic manipulation systems [3]. The use of robotic manipulators has proven to be advantageous for employing new deposition strategies that do not rely on the common slicing techniques used for the powder bed fusion processes. The part or the head can be inclined during the process to follow continuous 3D scan trajectories making it possible to generate complex geometries without the need of support structures [4,5]. However the major drawbacks are the low dimensional accuracy of the robotic system and the poor surface finish resulting from the layer-wise nature of AM processes, as well as the presence of sintered particles on the surface [6,7]. Therefore, post-processes are usually needed to comply with the geometrical and mechanical requirements.

Several works have shown the influence of processing conditions on the surface quality of LMD produced parts [8–10]. The surface roughness along the build direction commonly remains at very high values (R_a =20-30 μm and S_a=20-30 μm) for many of the engineering applications. For instance, a rough turning or milling operation would typically

produce an average surface roughness in the range of R_a=1-2 μm [11]. Hence, in industrial applications the surface quality of LMD produced parts requires finishing steps, which increase production time and costs [12] [13]. The geometrical flexibility of the LMD process with robotic manipulation systems increases the geometrical complexity of the parts, which also renders the finishing process more difficult. Undercuts and regions that are difficult to reach may limit the use of mass finishing processes as well as chip removal post processing.

The use of hybrid approaches to deposit and finish the workpiece within the same machine is an appealing approach for LMD processed parts to resolve finishing issues related to complex geometries [14]. The machining process can also be used to correct the geometrical deviations if the material allowance is sufficient. On the other hand, process planning between additive and subtractive processes should be carefully applied to the accessibility of the machined regions. The use of laser re-melting as a surface polishing operation is another solution that is intrinsically available to the LMD system. The same laser source used for the deposition process can be employed to polish the surface by re-melting [15–18]. Concerning additively manufactured components, the use of laser re-melting has been explored more widely for products obtained using powder bed fusion techniques. Despite its high potential to finish complex part geometries, the use of laser re-melting with LMD produced products still requires further attention [19,20].

One of the issues concerning the finishing of LMD produced surfaces relates to the difficulty in characterizing them. Such surfaces are composed of complex features such as high slopes, undercuts and changes in optical properties that makes it challenging for the measurement instruments to recreate the roughness profile dataset [21]. Moreover, the presence of strong anisotropy given either by the visible layers in vertical surfaces or different tracks in horizontal ones, imposes the necessity to employ 3D acquisitions to obtain a meaningful description of the surface topography [22].

Different and highly detailed standards have been developed over the years to analyse the roughness and waviness of conventionally manufactured surfaces [23–25]. However, the applicability of these standard surface roughness measurement parameters to additively manufactured complex surfaces is still limited [26]. The use of areal surface roughness measurements, texture analysis methods, and techniques in spectral domain seems to be more appropriate for such purposes [27–29]. Indeed, a point that requires attention concerning laser re-melting is the fact that this finishing process may also produce a new surface texture. While lowering the roughness and waviness amplitudes of the surface, laser re-melting can also generate a new texture, which can degrade the surface quality.

In literature, the capability of laser re-melting to reduce the surface roughness has been proven when applied to bulky components [30–32] and thin-walled structures [33]. The re-melting process has also been proposed for modifying and tailoring the microstructure of LMD parts [34]. However, the laser re-melting process has mostly been performed with the use of separate laser sources and/or machines from that used for deposition or it has been performed in a separate step. The effects of the interaction between material and laser beam during the re-melting process have been analysed by Ramos et al. [35]. The authors defined two different working conditions namely, Surface Shallow Melting (SSM) and Surface Over Melting (SOM). The transition zone between the two conditions was the one capable of obtaining the best results in terms of surface roughness reduction. Mathematical models have also been developed to predict the laser-material interaction in the re-melting process [36]. However, the efficacy of these models for predicting the final surface topography is limited due to complex multi-physics phenomena.

An overall analysis of literature shows the need for combining surface characterization and process knowledge to develop a laser re-melting process for finishing needs of freeform LMD components. Accordingly, this work analyses the laser re-melting process applied to thin-walled tubular AISI 316L stainless steel parts produced by LMD. A robotic LMD system was used for both the deposition and the re-melting phases, with a view to adapting this process for freeform structures. Within the work, areal surface measurements were used along with the power spectrum of the surface to understand the texture formation. In particular, the filtering stages were defined to employ the conventional S_a parameter along with a non-conventional waviness parameter on the areal data. An experimental campaign was conducted including the main laser re-melting process parameters, such as laser power and overlap, as well as parameters used to assess the feasibility of reaching restricted zones by employing different scan strategies and inclination angles with a robotic system. The experimental work was conducted to minimize surface roughness and waviness together, while not producing a new surface texture. Finally, the use of re-melting on more complex geometries starting from the optimal results on simple geometries was discussed.

2. EXPERIMENTAL SETUP AND METHODOLOGY

2.1 Robotic LMD system and material

Figure 1 shows the robotic LMD system, namely AddiTube, developed for large area deposition with high geometrical flexibility (BLM Group, Cantù, Italy) [5]. The deposition head positioning was carried out by a 6-axis anthropomorphic robot (ABB IRB 4600-45, Zürich, Switzerland), while a 2 degree freedom positioner (ABB IRBP A-250, Zürich, Switzerland) manipulated the workpiece synchronously. The laser source used was a multimode fibre laser with 3 kW maximum power output (IPG YLS-3000, Cambridge, MA, USA). The laser source was equipped with a 50µm feeding fiber connected to a 400µm process fiber through a fiber-to-fiber coupler. The process fiber was connected to a deposition head (Kuka Reis MWO-I, Obernburg am Main, Germany) with a mobile 100 mm collimating lens and a 200mm focal lens. A 3-jet powder nozzle was mounted on the deposition head (Fraunhofer ILT, 3-JET-SO16-S, Aachen, Germany). A double-barrel powder feeder (GTV, Twin PW 2/2- MF, Luckenbach, Germany) was employed. Gas atomized AISI 316L powder was used throughout the work with a particle size distribution corresponding to D10= 45 and D90= 90µm (LPW Technology, Runcorn, United Kingdom). Argon was used both as carrier and shielding gas. Programming of the deposition and re-melting trajectories was carried out by means of Robot Studio software (ABB, Zürich, Switzerland). The main characteristics of the system are shown in Table 1.

Table 1 Main characteristics of the system.

Parameter	Value
Operating volume	1.5x1.5x1.5 m^3
Laser wavelength, λ	1070 nm
Laser maximum power, $P_{,max}$	3000 W
Fiber diameter, d_f	400 µm
Focusing lens, f_f	200 mm
Collimation lens, f_c	129 mm

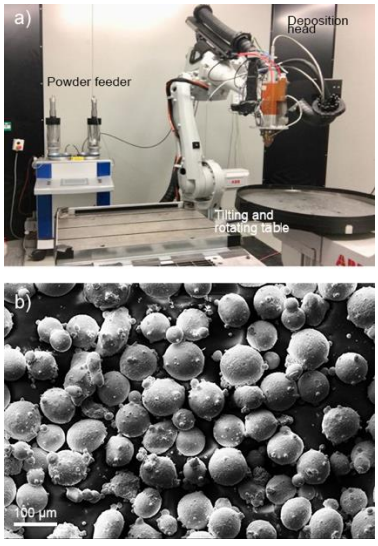

Figure 1 LMD configuration with robotic system and SEM image of used 316L powder

2.2 LMD of the thin-walled tubular structures

To study the effects of laser re-melting, the deposition step was fixed to obtain equal samples before performing the surface treatment. A thin-walled cylindrical shape was chosen as representative of thin walled structures with a height of 40mm and a diameter of 35mm. The deposition was performed with the use of a spiral strategy starting with the deposition of a first layer and then increasing for a height equal to the layer thickness for each round. The process

parameters were set based on a previous work, making it possible to produce relatively small values of surface roughness for the LMD process along with high apparent density (>99.5%) and reasonable productivity [15]. The parameters used for the deposition process are listed in Table 2.

Table 2. Laser metal deposition process parameters.

Parameter	Level
Laser power, P	370 W
Scan speed, v	22 mm/s
Layer thickness, z	0.25 mm
Laser spot diameter, d_s	1.1 mm
Stand-off distance, SOD	10 mm
Powder mass flow rate, $\dot{m}$	9.2 g/min
Shielding gas flow rate, FR	25 l/min

2.3 Surface characterization

2.3.1 Acquisition and filtering

Focus variation microscopy was used to acquire the surface topography (Alicona Infinite Focus, Graz, Austria). An area of 10 mm x 10 mm of the external surface of the tube was acquired. Given the features of additively manufactured surfaces such as high slopes, undercuts and varying optical properties, the acquisitions were performed with the use of polarized light and a 10x magnification lens. The numerical aperture of the lens was 0.3 with 0.88 µm lateral sampling distance in a 1429X1088 μm^2 field of view. In the current configuration vertical and horizontal resolutions were set to 0.9µm and 3.5µm respectively.

A summary of the filtration steps applied and pseudo-colour images of the obtained surfaces is visible in Figure 2 [37]. A high-pass areal Gaussian S-filter with a nesting index value of 0.02mm was applied at first [38] followed by an F-operation step (or form removal process) where a cylindrical form was subtracted to the acquired data ending up in the so called S-F surface. This obtained S-F surface was used for the subsequent topography and frequency domain analysis. In laser re-melting the process is known to eliminate the high frequency components, while generating low frequency ones. Accordingly a single indicator cannot be adequate for an optimization process. Hence, a further filtration step (L-filter) was applied to distinguish between the short scale lateral components forming the standardized S-L surface and the long scale components forming the non-standardized L-F surface. The two scale-limited surfaces obtained were used to calculate the arithmetical mean height parameters: $S_{a,SL}$ for the S-L surface and $S_{a,LF}$ for the L-F surface. These parameters are analogous to R_a roughness and W_a waviness parameters employed in linear measurements. Accordingly, the cut-off value for the L-filter was set to 0.8mm to allow a closer comparison with the more common linear roughness and waviness parameters commonly used in literature [25]. In this work $S_{a,SL}$ and $S_{a,LF}$ parameters are referred to as average surface roughness and average surface waviness conveniently.

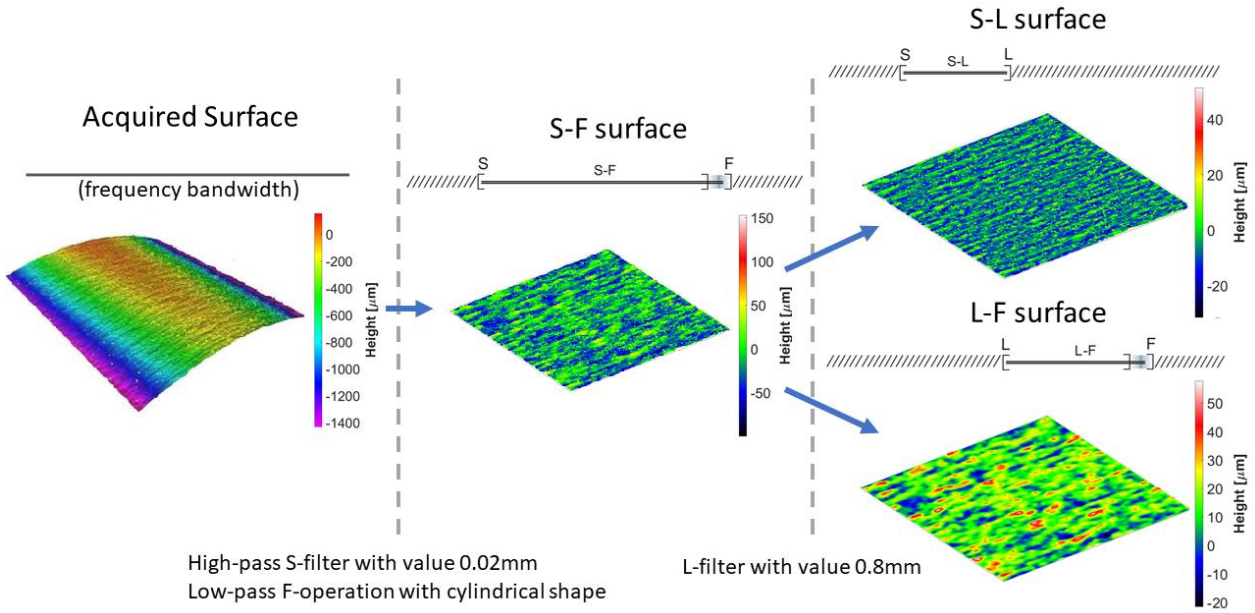

Figure 2 Summary of the filtration steps (dashed lines) needed to obtain the S-F surface and S-L surface defined in ISO 25178-3 as well as L-F surface. Over each surface a visual representation with different colour bar scales is provided of the remaining frequency bandwidth after the filtration steps.

2.3.2 Frequency domain analysis

The acquired surface data was analysed in the frequency domain as well. As shown by Hafiz et al. [39], an analysis in the frequency domain can distinguish between the contributions of the different wavelength components generated by different physical phenomena. Despite being a well-known operation for characterizing surface measurements [42][43], the use of the power spectrum with 3D surface measurements of additively manufactured surfaces in literature has been limited [44]. This approach has been found to be useful during the characterization of surface textures [40] as well as laser re-melted surfaces [41].

S-F surfaces were used for calculating the power spectrums in both x and y directions for the measurement corresponding to the circumferential and axial directions. To calculate the power spectrum, the discrete Fourier transform was used. For each spatial frequency f, the Fourier coefficient was calculated along a chosen x direction. Each array of the matrix dataset of z heights with N number of points were employed, where k indicates the index of each measured point. The corresponding Fourier coefficient C_F is computed using the following equation.

$$C_F = \frac{1}{N}\sum_{k=0}^{N-1} z(x_k) e^{i2\pi\frac{kf}{N}} \tag{1}$$

Once the Fourier coefficients are calculated, each value of the power spectrum S_{CC} is calculated using the following equitation:

$$S_{cc} = C_F^* \, C_F \tag{2}$$

where C_F^* is the complex conjugate of C_F. To calculate the power spectrum of the S-F surface along a specific direction all the power spectrum of parallel arrays along the chosen direction were averaged. The power spectrum was calculated for both axial and circumferential directions on the cylindrical specimens to identify texture formation on these two main directions. The transfer function between the re-melted and as-deposited surface M_n was calculated by:

$$M_n = \frac{C_{2,F}}{C_{1,F}} \tag{3}$$

where $C_{2,F}$ and $C_{1,F}$ are the Fourier coefficients of the re-melted and as-deposited surfaces related to the same wavelength n. If the value of the transfer function M_n is higher than 1 in a frequency range, it means that the contribution to the roughness given by those wavelengths has increased during the surface treatment with a detrimental effect on surface quality. On the other hand, where the transfer function is lower than 1 it means that those contributions were smoothed by the process. In a first approximation an optimal surface re-melting process should be based on SSM, producing M_n values less than 1. Process conditions producing SOM are likely to produce M_n values higher than 1 due to the formation of a new surface texture perpendicular to the re-melting path.

3. STUDY OF LASER RE-MELTING ON THIN-WALLED TUBULAR STRUCTURES

3.1 Laser re-melting strategies

Laser re-melting was performed with varying scanning strategy and process parameters to study the effect and interaction in the surface quality improvement obtained. At the end of the deposition, the tilting axis of the workpiece positioner was rotated by 90° to place the tube in a horizontal direction and perform the re-melting on top external surface of the horizontally oriented tube.

Given the geometry of the component two main possible strategies were defined, whose schematic representations are visible in Figure 3:

- Spiral trajectory: The laser path follows the circumference of the tube moving along the axial direction for a distance equal to the defined hatch spacing for each round. In this case the laser is kept on for the whole length of the process.
- Axial trajectory: The laser path follows the axis of the tube with mono-directional scanning. To reduce thermal distortions equally spaced tracks are performed for each rotation of the tube. In this case the laser is continuously turned on and off during the surface treatment resulting in lower overall heating of the part.

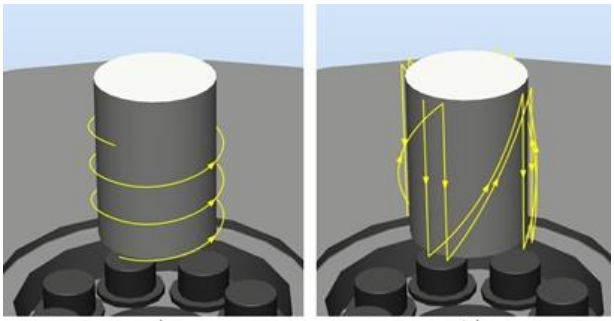

Figure 3 Schematic magnified representation of a) spiral scanning strategy b) axial scanning strategy

3.2 Experimental design

To calculate a second order model of the effects of process parameters on surface quality, a Central Composite Design (CCD) experimental campaign was planned. Scan speed (v) was fixed at the maximum level provided by the system to maintain productivity. The laser spot diameter (d_s) was enlarged to 2.5 mm defocusing by 12 mm from the focal plane to generate a wider and shallower melt pool. Hence, the stand-off distance (SOD) was increased compared to the deposition phase. The shielding gas flow rate (FR) was kept at the same level as the deposition phase. Only a single pass (N) was applied in the re-melting phase. The varied parameters were selected to allow for flexible regulation on more complex geometries as well. During the deposition of more complex thin-walled structures it can be expected that the laser incidence angle (θ) must be varied due to reduced accessibility. On the other hand, laser power (P) and track overlap (O) can be varied to maintain a lower roughness with the accessibility limitations given. The levels of

the varied parameters were set through preliminary experiments, which are not reported here for the sake of brevity. As shown in Table 3 the laser power was varied between 300 and 400 W corresponding to a region with lower and higher power values compared to the deposition phase. Combined with a larger beam and a higher scan speed, the melting occurs only at a superficial level. The overlap between adjacent re-melted tracks is calculated employing the following formula

$$O = \left(1 - \frac{h}{d_s}\right) 100 \tag{3}$$

where d_s is the laser spot size and h is the hatch distance between adjacent tracks. The incidence angle is shown in Figure 4. It can be noted that the same incidence angle can be achieved by positioning the workpiece in different directions. Throughout the re-melting experiments the workpiece axis was kept in the horizontal direction (as in Figure 4.b). As responses of the experimental campaign both areal average roughness $S_{a,SL}$ and $S_{a,LF}$ parameters were used. Power spectra were also calculated to reveal the presence of the periodic components.

Table 3 Details of the CCD experimental design with α =±1.633. Axial points are shown with a, corner points with c and centre values with 0.

Fixed parameters	**Level**				
Scan speed, *v*	55 mm/s				
Stand-off distance, *SOD*	29.5 mm				
Laser spot diameter, d_s	2.5 mm				
Number of passes, *N*	1				
Shielding gas flow rate, *FR*	25 l/min				
Continuous varied parameters	**Levels**				
	-a	-c	0	+c	+a
Laser power, *P* [W]	300	319	350	381	400
Overlap, *O* [%]	50.0	57.8	70.0	82.2	90.0
Angle, θ [°]	45.0	53.7	67.6	81.3	90.0
Categorical varied parameters	**Levels**				
Strategy	Spiral		Axial		

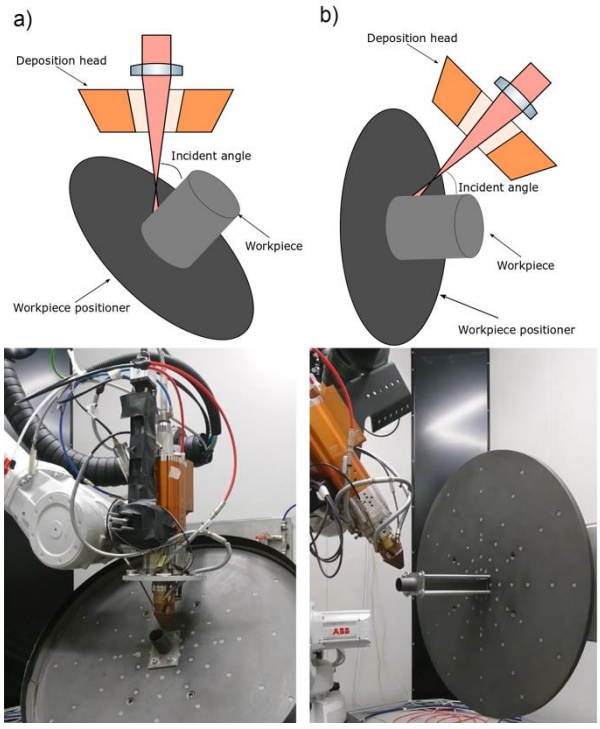

Figure 4 Scheme of re-melting configurations where an equal laser incidence angle is achieved a) rotating the workpiece and b) deposition head and placing the workpiece in the horizontal direction.

4. RESULTS

4.1 As-deposited surface

Figure 5.a reports an example of the as-deposited specimen, while a pseudo-colour image of the surface morphology can be seen in Figure 5.b. The process capability for the areal roughness $S_{a,SL}$ and waviness $S_{a,LF}$ parameters were identified as average values ± three-times the sample standard deviation (μ± 3σ) as an industrial indicator for process stability [45]. Measurements were averaged over 5 samples: $S_{a,SL}$ and $S_{a,LF}$ values were found to be $10.35 \pm 0.42\ \mu m$ and $9.57 \pm 0.48\ \mu m$ respectively. These values also corresponded to a 95% confidence interval for the mean at 10.20-10.52 μm and 9.41-9.72 μm for $S_{a,SL}$ and $S_{a,LF}$ respectively. The low dispersion of the measurements points to a stable and repeatable deposition process which makes it possible to compare the results obtained after the surface treatment with the initial samples used as a reference condition. The calculated power spectrum of the as-built surface visible in Figure 5.c points to:

- An overall higher amplitude of the roughness spectrum components along the axial direction with respect to the ones along the circumferential direction of the tubes, pointing to an anisotropy in surface roughness.
- The strong influence of the layering technique of the AM process visible along the axial direction (which corresponds to the building direction). As expected, the peak frequency is equal to $4mm^{-1}$ since it is related to a deposited layer thickness of $0.25mm$.

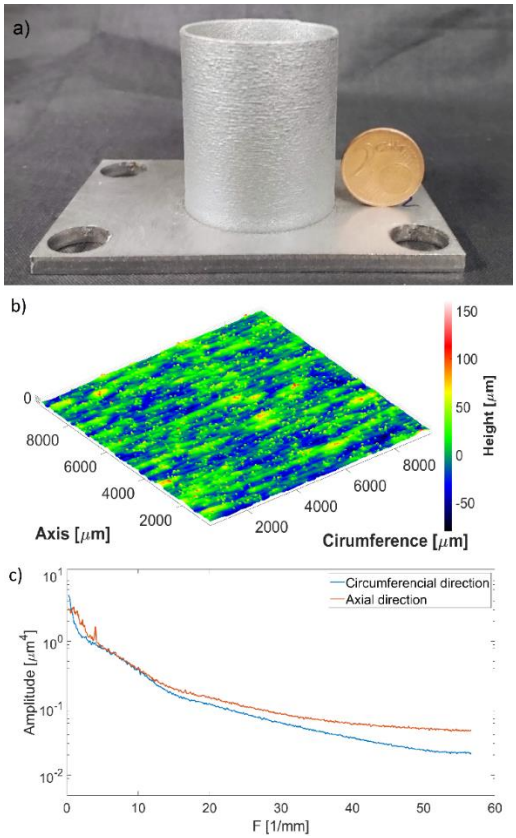

Figure 5 a) Macrograph of the as-deposited tube with visible layers and powder particles sticking on the surface. b) Pseudo-colour image of the acquired surface topography. c) S-F surface power spectrum where a peak is visible for the component related to the layers with wavelength 0.25mm

4.2 Roughness and waviness after re-melting

The broad processing window analysed throughout the central composite design (CCD) experimental plan allowed us to work in either SSM or SOM conditions as a function of the energy input, which mainly depends on laser power and

overlap, and is further affected by the re-melting scanning strategy used. Because of the imposed surface topography modification, which is well depicted by the calculated transfer functions, the obtained surface roughness and waviness can vary significantly from a strong reduction to an increase compared to the initial condition. Throughout the experimental campaign the minimum and maximum values obtained with different process parameters ranged from 1.82µm to 9.42µm for $S_{a,SL}$ and from 3.97µm to 19.11µm for $S_{a,LF}$. An overview of the effects of the process parameters on surface roughness $S_{a,SL}$ obtained after the re-melting process is visible through the main effect and interaction plots (see Figure 6).

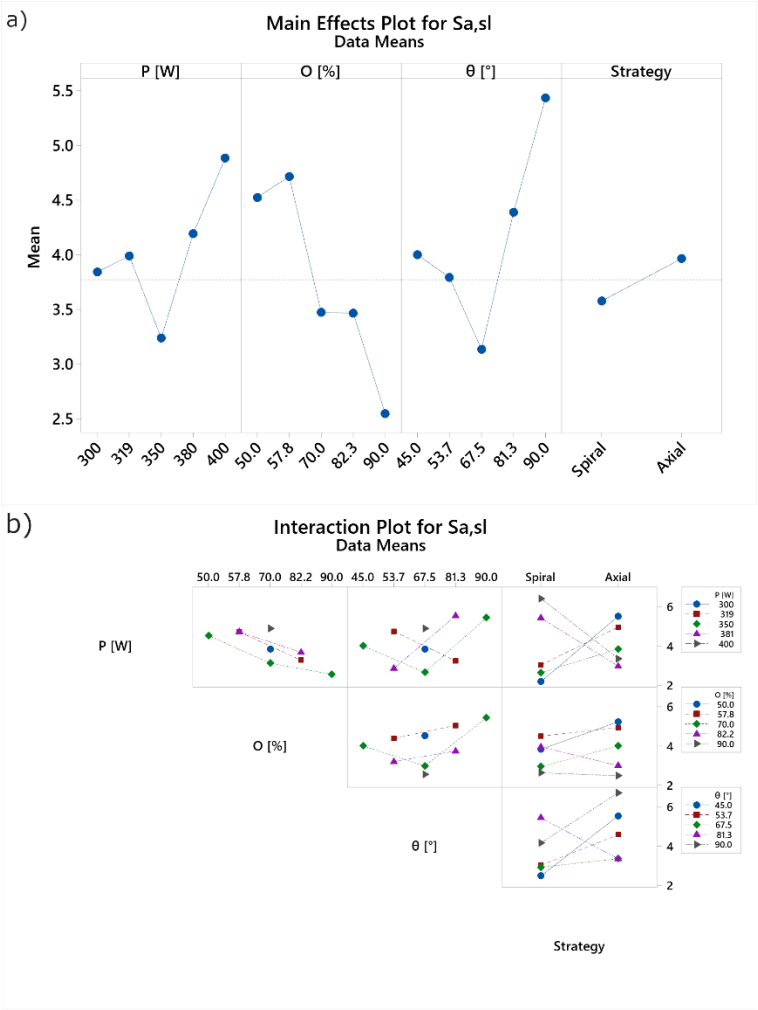

Figure 6 a) Main effects and b) interaction plots for $S_{a,SL}$ obtained after laser re-melting

The results show that all the parameters are expected to have strong interactions with one another. The use of a spiral strategy with a high overlapping value was required to reduce the roughness $S_{a,SL}$ value. On the other hand, laser power and incidence angle are expected to present a strong parabolic behaviour with worst results at both borders of the respective processing window and highest roughness improvements close to the centre value used.

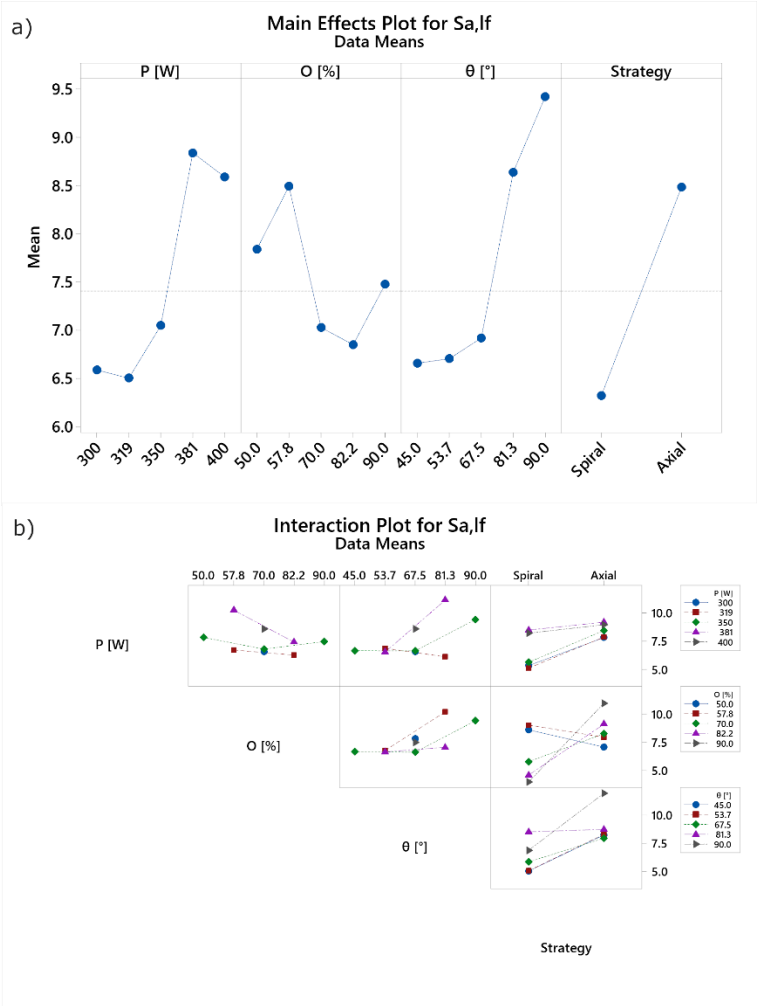

Figure 7. a) Main effects and b) interaction plots for $S_{a,LF}$ obtained after laser re-melting

As for the waviness value, an overview of the effect of the process parameters on the surface waviness obtained after the re-melting process is visible in the main effect and interaction plots (see Figure 7). In contrast to the results obtained for the surface roughness, the lower values of laser power and incidence angle tend to show better results, while the overlap shows a reduction in surface waviness in the whole processing window. Regarding the strategy, as for the roughness, the use of a spiral trajectory was found to end up giving a better surface quality.

4.3 Peak wavelength shift

Table 4 shows a close up in the low frequency range of the power spectrum of three example surfaces obtained using different process parameters. While the amplitude of the generated principal periodical component can be mainly related to the laser power used, the wavelength of the visible peak is found to be related to the re-melting scanning strategy and overlap used. In particular, a ripple direction was found perpendicular to the laser beam tracks' direction upon the surface. The ripples formed in the circumferential direction in the case of an axial trajectory and in the axial direction in case of a spiral trajectory. On the other hand, the value of the imposed wavelength, measured from the frequency value of the peak present in the power spectrum, was equal to the scan hatch distance between adjacent tracks during laser re-melting as seen in Figure 8. This relationship between scan strategy used and topography generated may make it possible not only to use laser re-melting as a smoothing process, but also to use it for the imposition of a desired surface structure with predictable amplitude and wavelength.

Table 4. Characteristic S-F surface power spectra with different process parameters. a) Low frequency peak in the circumferential direction, b) low frequency peak in an axial direction, c) high frequency peak in the axial direction

	S-F surface power spectrum	Process parameters and generated surface structure
a)	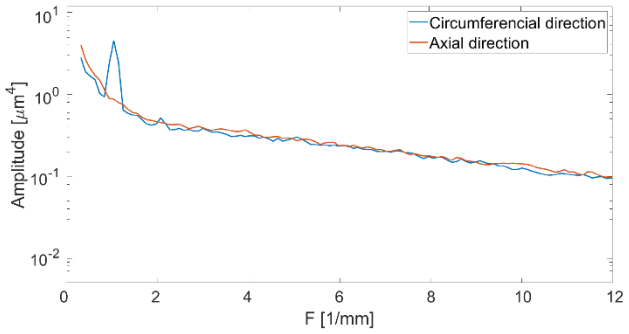	P= 350 W O= 57.8 % θ = 81.3° Strategy: axial h=1.055 mm Pw= 1.002 mm^{-1} = 0.998 mm
b)	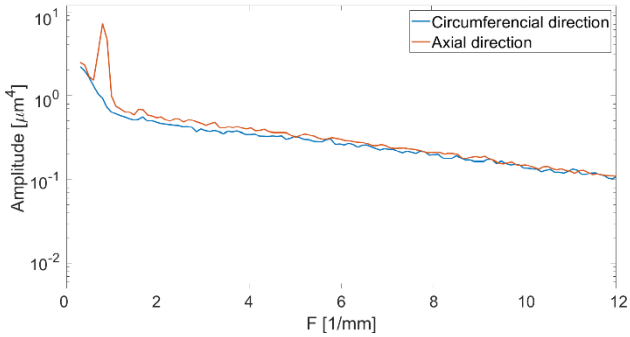	P= 350 W O= 50.0 % θ= 67.5° Strategy: spiral h=1.250 mm Pw= 0.786 mm^{-1} = 1.272 mm
c)	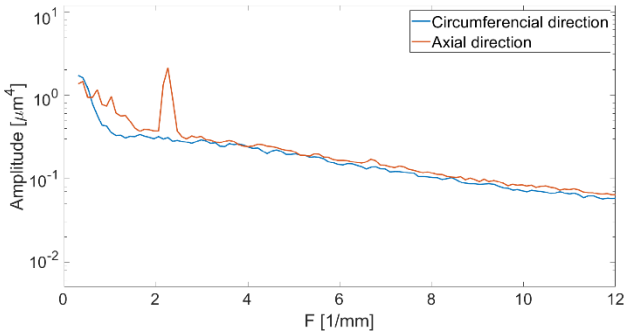	P= 319 W O= 82.2 % θ= 81.3° Strategy: spiral h=0.445 mm Pw = 2.252 mm^{-1} = 0.444 mm

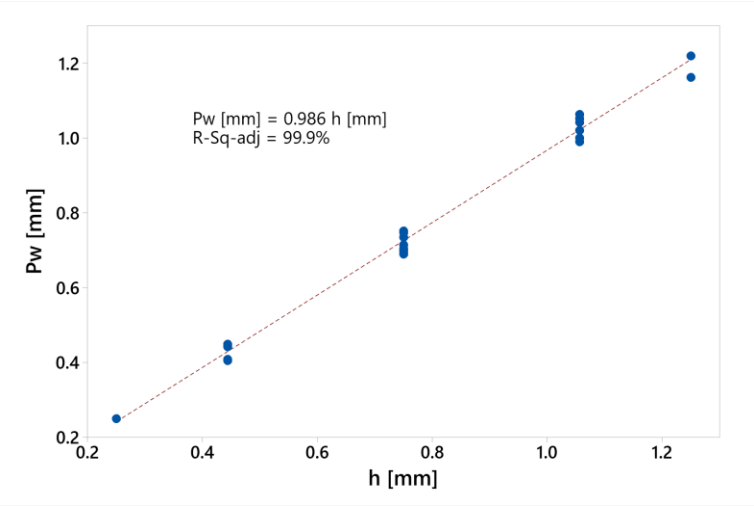

Figure 8 Direct relationship between the hatch distance (*h* [mm]) between laser tracks, which is controlled by the overlap parameter and the peak wavelength (*Pw* [mm]) measurement in the power spectrum.

4.3 Re-melted surface topographies

In the experimental campaign, both surface shallow melting (SSM) and surface over melting (SOM) occurred as shown in Table 6. The different results can be better depicted by looking at the power spectrum for the re-melted surfaces and at the calculated transfer functions compared to the as-deposited condition shown in Table 6.

When low laser power and overlap are employed, the energy input was not high enough to generate a stable melt pool, an SSM condition occurs and the topography is only slightly modified compared to the initial structure. Consequently, this result is visible in the calculated transfer function which has a value very close to 1 in the whole frequency domain, meaning a similar topography to the LMD as-deposited surface. On the other hand, when the SOM condition occurs a completely new topography is imposed with a strong waviness pointed out by the presence of peaks in the power spectrum. The topography changes imposed by the re-melting process compared to the as-deposited surface are visible in the calculated transfer function that has very low values in the high frequency range but is characterized by the presence of low frequency components with values greater than 1, meaning that the amplitudes of the power spectrum at that wavelength are higher than the ones of the as-deposited surface at the same wavelength.

These results show that the effect of laser re-melting on the surface topography, and as a consequence on the measured roughness parameters, has a strong dependency on the analysed wavelength range. The higher frequency components can be either slightly modified or reduced by up to 80% compared to their initial values and are usually characterized by an almost constant value. On the other hand, the it is more challenging to reduce the lowest frequency components, as they have an average improvement of up to 50% and they can be characterized by the presence of peaks with values greater than 1 when working with an energy input much higher than the optimal conditions.

Only when the combination of the laser power and overlap are in the correct range, does the newly imposed topography have all the spectral components much lower than those for the as-deposited surfaces.

Table 5 Pseudo colour images of surfaces obtained after laser re-melting with different sets of process parameters. The characteristics of a) SSM, b) SOM and c) SSM-SOM transition zones are visible from the surface texture.

a)	b)	c)
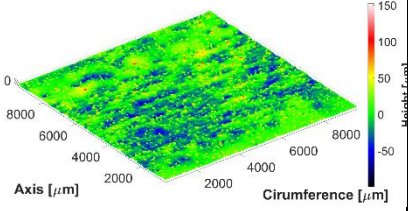	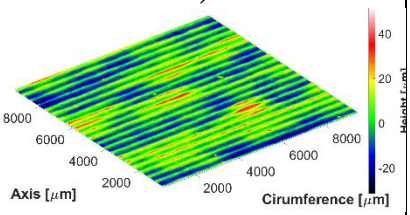	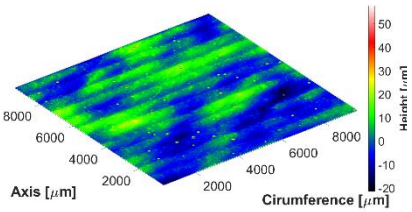
P= 319 W O= 70.0 % θ= 45.0 °	P= 400 W O= 57.7 % θ= 81.3°	P= 319 W O= 82.2 % θ= 81.3°

Table 6 Frequency domain analysis of the three surfaces in Table 5. a) Condition of SSM where topography is only slightly modified b) Condition of SOM where a new topography with high waviness is imposed c) SSM-SOM transition zone where the roughness profile is smoothed in the whole wavelength domain. The dashed line on the transfer function plots depict no change compared to the as-built surface.

	FFT of re-melted surface	Re-melting process transfer function
a)	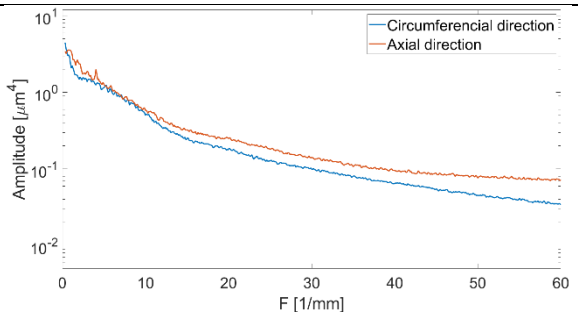	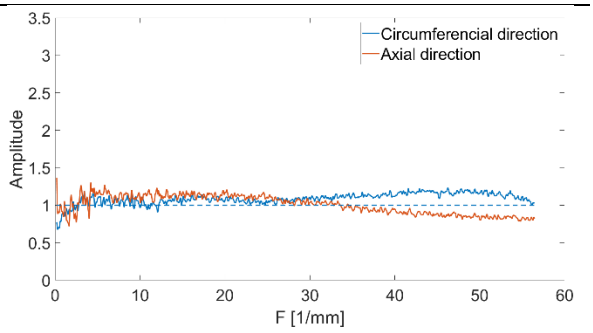
b)	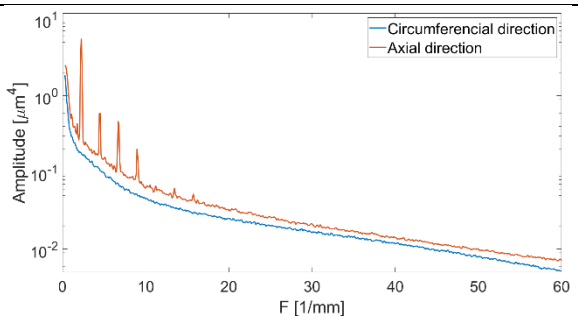	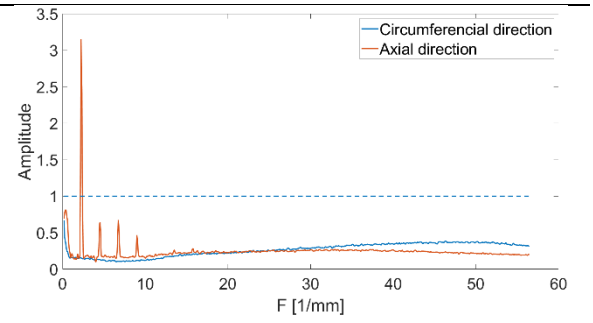
c)	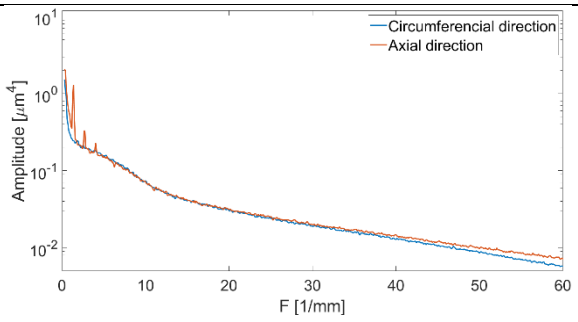	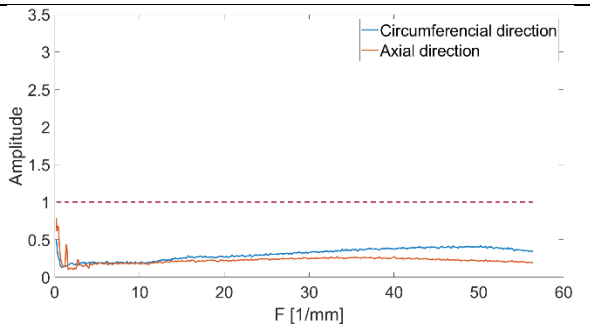

4.4 Optimization of the process parameters for minimizing $S_{a,SL}$ and $S_{a,LF}$

The experimental data was used to fit second order regression equations. The statistical significance levels were set at α=0.05. Box-Cox transformation was applied to ensure normality of the residuals. For surface roughness $S_{a,SL}$ a transformation of $y^{-0.5}$ was found adequate, while for waviness $S_{a,LF}$ $1/y$ was found to be suitable. The adequacy of the model expressed, with simplified ANOVA tables for the two process, can be viewed further in Table A. 1. It can be noted that all parameters are significant either at the main effects, second order or interaction level. Concerning the surface roughness, laser power, track overlaps and laser incidence angle are strongly significant in a non-linear manner. Laser power appears to have a strong interaction with strategy, as high levels of power tend to produce lower roughness with an axial strategy, while lower power is required for a spiral strategy. Power and incidence angle also interact in a strong manner, while strategy has weaker interactions with overlap and incidence angle. Concerning surface waviness, the parameters appear to have a stronger impact at a main effects level than on the second order. Power and incidence angle as well as overlap and strategy have strong interactions.

Since all the statistical hypotheses were verified, the models did not show lack-of-fit and the R^2_{adj} were reasonably high, and so no further model reduction was carried out. In Table 7 the coefficients of the fitted equations are shown. For both the outputs, the equations are shown separately for the two levels of the categorical factor (strategy).

Table 7 Coefficients of the regression equation obtained fitting $S_{a,SL}$ and $S_{a,LF}$ values for both spiral and axial strategies

Parameter	$S^{-0.5}_{a,SL,spiral}$	$S^{-0.5}_{a,SL,axial}$	$S^{-1}_{a,LF,spiral}$	$S^{-1}_{a,LF,axial}$
Constant	13.38	15.33	-2.130	-2.081
Power	-0.0543	-0.0580	0.00925	0.00960
Overlap	-0.0520	-0.0564	0.00185	-0.00226
Angle	-0.0962	-0.1006	0.02003	0.02085
Power2	$6.6 * 10^{-5}$	$6.6 * 10^{-5}$	$-1.0 * 10^{-5}$	$-1.0 * 10^{-5}$
Overlap2	$3.13 * 10^{-4}$	$3.13 * 10^{-4}$	$-3.2 * 10^{-5}$	$-3.2 * 10^{-5}$
Angle2	$3.78 * 10^{-4}$	$3.78 * 10^{-4}$	$-5.1 * 10^{-5}$	$-3.78 * 10^{-5}$
Power $*$ Overlap	$1.7 * 10^{-5}$	$1.7 * 10^{-5}$	$1.0 * 10^{-5}$	$1.0 * 10^{-5}$
Power $*$ Angle	$1.36 * 10^{-4}$	$1.36 * 10^{-4}$	$-4.8 * 10^{-5}$	$-4.8 * 10^{-5}$
Overlap $*$ Angle	$1.7 * 10^{-5}$	$1.7 * 10^{-5}$	$3.7 * 10^{-5}$	$3.7 * 10^{-5}$

The desirability function was used for the optimization of the two process outputs together [46]. The approach uses the estimations provided by the regression equations and calculates a numerical value between 0 and 1, namely the desirability of the given configuration of the parameters. The desirability function d_i for minimizing a process output is defined as the follows.

$$d_i = \begin{cases} 1 & y_i < T \\ \left(\frac{U - y_i}{U - T}\right)^w & T \leq y_i \leq U \\ 0 & y_i > U \end{cases} \quad (4)$$

where, T represents the target value for the i^{th} response y_i, U represents the acceptable upper limit and w is the weight given to each response. Desirability values closer to 1 are closer to the expected outcome, while those close to 0 are far from it. In the case of two responses of a process such as in this case, a composite desirability function D can be calculated:

$$D = (d_1 \cdot d_2)^{1/2} \quad (4)$$

where d_1 and d_2 are the two desirability functions of each output. Also in this case the composite desirability values closer to 1 provide solutions close to the desired value.

For this specific case, for both $S_{a,SL}$ and $S_{a,LF}$, U was set to the maximum value measured throughout the experimental campaign while T was set to the minimum value predicted by the fitted regression equations. Both responses were given the same weight w equal to 1 to calculate the composite desirability. Using the second order regression equations calculated for both $S_{a,SL}$ and $S_{a,LF}$ and the desirability function for response minimization shown in Equation 4, it was possible to find the parameters' values within the processing window used, capable of minimizing roughness and waviness at the same time.

In these conditions, the optimization output for the single and composite desirability functions can be seen in Figure 9. The optimal parameters for minimizing both outputs were P= 333W, O= 79%, θ= 66° and spiral strategy with a composite desirability of D=0.9765. The parameter set predicted $S_{a,SL}^{pre}$= 2.20 µm and $S_{a,LF}^{pre}$=4.04 µm.

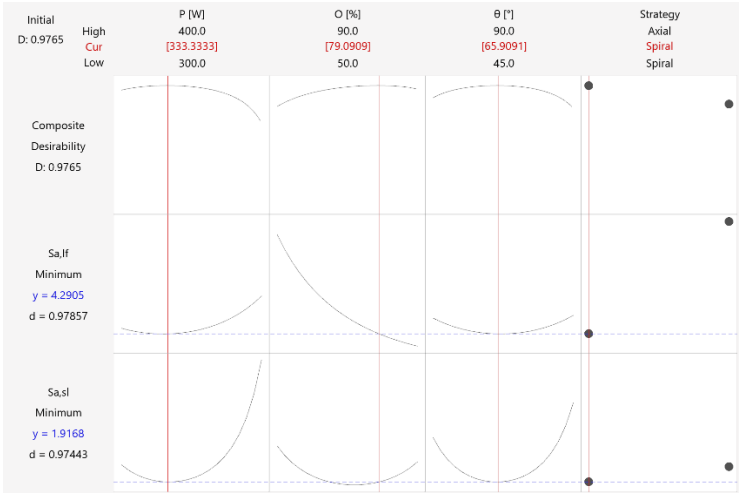

Parameter	Level
Laser power, P [W]	333
Overlap, O [%]	79
Angle, θ [°]	66
Strategy	Spiral

Figure 9 Result of desirability functions for mutual minimization of $S_{a,SL}$ and $S_{a,LF}$ and the table of the optimized parameter set.

With the processing conditions found, three validation tests were performed. Figure 10.a shows an example of the cylindrical specimens produced. The power spectrum shown in Figure 10.b indicates that the optimized conditions did not produce any primary frequency in the power spectrum for the surface. The $S_{a,SL}$ and $S_{a,LF}$ measurements are shown in Table 9 along with the predicted values, confidence and prediction intervals. The mean values of $\bar{S}_{a,SL}$and $\bar{S}_{a,LF}$ are close to those expected and fall within the 95% confidence interval. All measured values lay within the 95% prediction -interval for the mean. It can be concluded that the optimization procedure via the use of the desirability function was successful.

Table 8 ***Measured values of roughness $S_{a,SL}$ and waviness $S_{a,LF}$ and their respective averages $\bar{S}_{a,SL}$ and $\bar{S}_{a,LF}$ compared to predicted values $S_{a,SL}^{exp}$ and $S_{a,LF}^{exp}$, confidence (CI) and prediction intervals (PI) derived from fitted models***

$S_{a,SL}$ $[\mu m]$	$\bar{S}_{a,SL}$ $[\mu m]$	$S_{a,SL}^{pre}$ $[\mu m]$	*95% CI*	*95% PI*
2.22 2.23 2.16	2.20	1.92	(1.65 ; 2.26)	(1.43 ; 2.97)
$S_{a,LF}$ $[\mu m]$	$\bar{S}_{a,LF}$ $[\mu m]$	$S_{a,LF}^{pre}$ $[\mu m]$	*95% CI*	*95% PI*
4.04 3.97 4.10	4.04	4.29	(4.00 ; 4.63)	(3.63 ; 5.24)

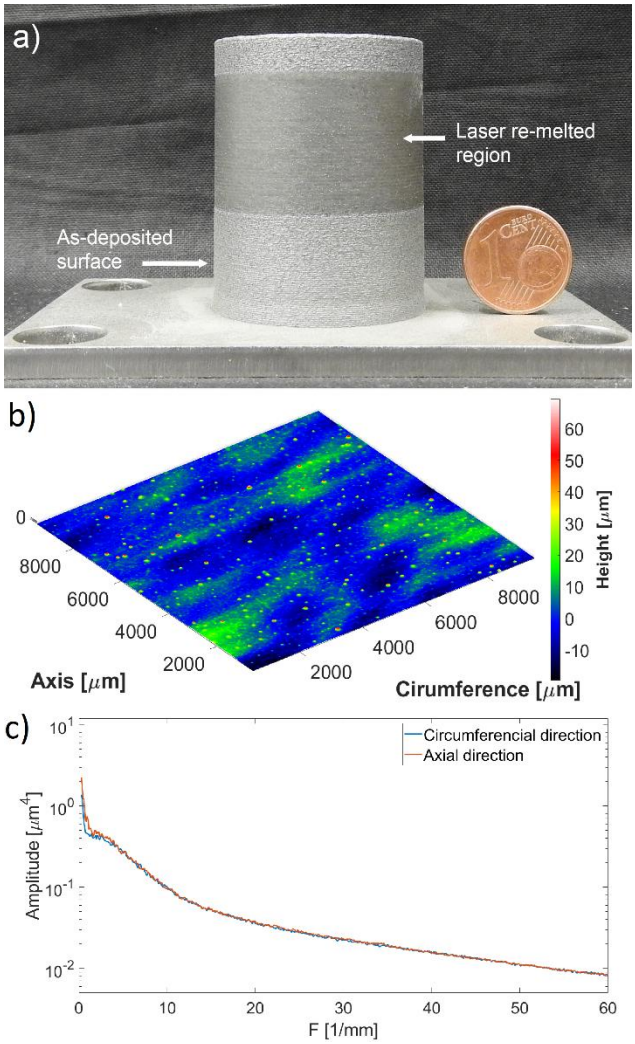

Figure 10 a) Macrograph of a sample obtained with the optimized laser re-melting parameters. b) Acquired surface topography. c) S-F surface power spectrum, which shows no dominant wavelength.

5. DISCUSSION

The results obtained show strong dependency of surface quality improvement on all four varied process parameters as well as on their interaction. Given the results obtained both in terms of measured roughness $S_{a,SL}$ and waviness $S_{a,LF}$

parameters and in terms of analysed surface topography, the main effects of each parameter on the surface topography obtained can be discussed.

- **Laser power**. This parameter directly affects the energy input provided during the process, determining the working condition to be either SSM or SOM. In optimal conditions the material redistribution occurs without the generation of any periodical surface structure, but for increasing values a ripple formation occurs where the waviness height increases together with the overheating of the surface.
- **Overlap**. Together with the laser spot diameter overlap determines the laser scan spacing which has been proven to be directly related to the wavelength of the generated periodical component. Depending on its value the frequency of the formed ripples can be either in the roughness or waviness frequency range. Hence, the overlap can strongly affect $S_{a,SL}$ and $S_{a,LF}$.
- **Laser incidence angle**. An interesting result arises from the advantages achieved by the use of an inclined laser that makes not only treating non-accessible surfaces with perpendicular lasers, but also improving the roughness reduction capabilities of the laser re-melting process possible. An inclined beam also results in an elliptical projection on the surface, which should reduce the beam intensity due to the beam enlargement on the inclined axis. Such a change in the beam shape also can increase the effective overlap between the adjacent tracks during the spiral re-melting strategy. Indeed the main effect of incidence angle follows a similar trend compared to the laser power, which confirms its effect on the laser irradiance. The interaction with the scanning strategy and overlap also confirms that the beam shape is effectively contributing the effective re-melted track width. The beam shape in focal position of the present optical configuration can be referred to as a quasi-top-hat distribution. Indeed, in the defocused conditions employed in the re-melting phase is expected to be uneven due to the use of the multimode fiber laser. The inclination of the beam with respect to the surface can help distributing the energy to a larger area hence obtain a more homogenous irradiance profile.
- **Scanning strategy**. When the geometry makes it possible for the surface to be re-melted, a strategy such as the spiral one, in which the laser is kept on for the whole length of the process, provides a more uniform result over the worked area. Monodirectional scanning strategies result in higher roughness $S_{a,SL}$ and waviness $S_{a,LF}$ especially close to the points where the laser is turned on and off. However, this strategy is more adaptable to virtually any surface shape.

The surface quality improvement given by laser re-melting is expected to be highly influenced by the heat dissipation properties of the treated surface and therefore by the part's material and geometry. The optimized conditions are limited to simple closed contoured, thin-wall geometries. For more complicated components, the process cycle should be planned to allow the re-melting process to intervene prior to the loss of access to the regions. Hence, the deposition process should be halted occasionally for the re-melting phase. The accessibility of the different zones depends on the deposited geometry, which determines the re-melting incidence angle and re-melting strategy. The developed regression equations should be resolved for each case, with the access restrictions, to provide the overlap and power values. Such solutions can be potentially implemented in the CAM software.

A key issue that remains open is related to the change in the initial surface topography as a function of the deposited geometry and the process parameters used. Indeed, the efficacy of the re-melting process depends on the initial surface quality. In the experimental conditions, the as-deposited components were characterized by a reasonably low surface roughness and waviness for the LMD parts, which made it possible to achieve surface roughness values comparable to a rough turning operation. Moreover, it is expected that the re-melting process will be sensitive to surface discontinuities and defects, which may arise from process instabilities as well as the deposited geometry. The use of increasingly common temperature feed-back control systems may improve the resilience of the process to such disturbances. This work concentrated on the outer surface of thin-walled parts with closed contours. Indeed, re-melting may be required for improving the quality of the inner walls of tubular structures. The applicability of re-melting depends on the accessibility of such zones. Indeed, careful programming of the deposition and re-melting phases would be required also taking the collision possibility into account.

Finally, productivity concerns should still be addressed. Within the entire experimental campaign, productivity varied between 0.03 and 0.25 m^2/h. In the optimal conditions a processing time of 76 s to work an area of 22 cm^2 was achieved corresponding to a productivity of 0.11 m^2/h. Although this may double the total production time, the possibility of carrying out the finishing operation on the same machine without the need for dedicated fixtures can ensure a significant reduction in the total lead time. These conditions are relevant for additive manufacturing, where single to small lot products are concerned.

6. CONCLUSIONS

This work shows the laser re-melting process applied to thin-walled cylindrical components produced by a laser metal deposition (LMD) robotic system. Tubular specimens were deposited, and their surfaces were re-melted with the same plant set-up assessing the feasibility of employing the method in view of complex geometries. The main conclusions of this work can be summarized as follows.

- The LMD produced parts are layered showing strong anisotropy beyond the highly irregular surface. The surface topography of LMD produced parts require the use of texture measurements as well as areal roughness and waviness parameters. In this work, the use of S-F surface for power spectrum, S-L surface for a roughness and the L-F surface for a waviness indicator were employed. The measurements were found complementary, providing the means for a better comprehension of the new texture formation and an effective optimization procedure.
- Laser re-melting conditions can effectively reduce the surface $S_{a,SL}$ roughness and $S_{a,LF}$ waviness. While these parameters are reduced, in SOM conditions, a new surface texture was formed. It was found that the peak frequency of the newly developed surface texture is correlated to the overlap between the re-melting tracks.
- In the optimal re-melting conditions, the areal roughness parameter $S_{a,SL}$ could be reduced by 79% together with a waviness $S_{a,LF}$ reduction of 58% with a low variation between the replications indicating a high process capability. Moreover, in the optimal conditions, no dominant spectral frequency was observed indicating an isotropic finish.
- Within the experimental campaign an empirical model was developed, which includes scan strategies and inclination angles. This empirical model can be integrated with a CAM software calculating the optimal parameters, and imposing the inclination angle and scan strategy required to approach different zones of the component.

While providing several aspects related to the applicability of the re-melting process, several other points were not addressed in this work. The effect of the process on bulky parts may be different due to the differences in thermal dissipation. The efficacy of the process on surfaces with a different as built finish may change. The results also imply the importance of the laser beam profile in the re-melting stage. Although the intention of this work has been to use the same laser beam for both deposition and finishing, the beam shape can be better fit for purpose also by implementing active beam shaping optics for an more even irradiance profile. Finally, the effect of the re-melting process on the geometrical accuracy may be important for thinner sections, which are more prone to thermal deformations.

7. ACKNOWLEDGEMENTS

The authors acknowledge the technical support from the BLM Group. This work was supported by the European Union, Repubblica Italiana, Regione Lombardia and FESR for the project MADE4LO under the call ”POR FESR 2014-2020 ASSE I - AZIONE I.1.B.1.3”. The Italian Ministry of Education, University and Research is acknowledged for the support provided through the Project "Department of Excellence LIS4.0 - Lightweight and Smart Structures for Industry 4.0”.

APPENDIX

Table A. 1 Simplified ANOVA table of the regression equations fitted to $S_{a,SL}$ and $S_{a,LF}$. Statistically significant coefficients are shown in bold.

p-value	$S_{a,SL}^{-0.5}$	$S_{a,LF}^{-1}$
Power	0.469	0.003
Overlap	**0.005**	**0.001**
Angle	0.110	**0.006**
Strategy	0.088	**0.000**
Power^2	**0.000**	**0.027**
Overlap^2	**0.003**	0.256
Angle^2	**0.000**	**0.026**
Power $*$ *Overlap*	0.680	0.451
Power $*$*Angle*	**0.001**	**0.000**
*Power*Strategy*	**0.000**	0.153
Overlap $*$ *Angle*	0.857	0.194
*Overlap*Strategy*	**0.037**	**0.000**
*Angle*Strategy*	**0.021**	0.132
Lack-of-fit	0.220	0.190
R^2_{adj}	73.5%	85.8%

REFERENCES

[1] Dass A, Moridi A. State of the Art in Directed Energy Deposition: From Additive Manufacturing to Materials Design. Coatings 2019;9:418. doi:10.3390/coatings9070418.

[2] Graf B, Gumenyuk A, Rethmeier M. Laser Metal Deposition as Repair Technology for Stainless Steel and Titanium Alloys. Phys Procedia 2012;39:376–81. doi:10.1016/j.phpro.2012.10.051.

[3] Ding Y, Dwivedi R, Kovacevic R. Process planning for 8-axis robotized laser-based direct metal deposition system: A case on building revolved part. Robot Comput Integr Manuf 2017;44:67–76. doi:10.1016/j.rcim.2016.08.008.

[4] Zhao G, Ma G, Feng J, Xiao W. Nonplanar slicing and path generation methods for robotic additive manufacturing. Int J Adv Manuf Technol 2018;96:3149–59. doi:10.1007/s00170-018-1772-9.

[5] Assaad M, Demir AG, Anilli M, Tamborini D, Mutti S, Molinari L, et al. Design and Pathway Programming of Freeform Thin-walled Geometries Produced by Laser Metal Deposition. Lasers Manuf. 2019, 2019, p. 1–10.

[6] Rombouts M, Maes G, Hendrix W, Delarbre E, Motmans F. Surface finish after laser metal deposition. Phys Procedia 2013;41:810–4. doi:10.1016/j.phpro.2013.03.152.

[7] Donadello S, Motta M, Demir AG, Previtali B. Monitoring of laser metal deposition height by means of coaxial laser triangulation. Opt Lasers Eng 2019;112:136–44. doi:10.1016/j.optlaseng.2018.09.012.

[8] Gharbi M, Peyre P, Gorny C, Carin M, Morville S, Le Masson P, et al. Influence of a pulsed laser regime on surface finish induced by the direct metal deposition process on a Ti64 alloy. J Mater Process Technol 2014;214:485–95. doi:10.1016/j.jmatprotec.2013.10.004.

[9] Gharbi M, Peyre P, Gorny C, Carin M, Morville S, Le Masson P, et al. Influence of various process conditions on surface finishes induced by the direct metal deposition laser technique on a Ti-6Al-4V alloy. J Mater Process Technol 2013;213:791–800. doi:10.1016/j.jmatprotec.2012.11.015.

[10] Zhang J, Shi S, Fu G, Shi J, Zhu G, Cheng D. Analysis on surface finish of thin-wall parts by laser metal deposition with annular beam. Opt Laser Technol 2019;119:105605. doi:10.1016/j.optlastec.2019.105605.

[11] CES EduPack 2017.

[12] Liebana F, Ukar E, del Pozo D, Lamikiz A, López de Lacalle LN, Etayo JM. Laser Polishing Operation for Die and Moulds Finishing. Adv Mater Res 2009;83–86:818–25. doi:10.4028/www.scientific.net/amr.83-86.818.

[13] Anilli M, Demir AG, Previtali B. Additive manufacturing of laser cutting nozzles by SLM: processing, finishing and functional characterization. Rapid Prototyp J 2018;24. doi:10.1108/RPJ-05-2017-0106.

[14] Cortina M, Arrizubieta JI, Ruiz JE, Ukar E, Lamikiz A. Latest developments in industrial hybrid machine tools that combine additive and subtractive operations. Materials (Basel) 2018;11. doi:10.3390/ma11122583.

[15] Bruzzo F, Catalano G, Demir AG, Previtali B. In-process laser re-melting of thin walled parts to improve surface quality after laser metal deposition. Key Eng Mater 2019;813 KEM:191–6. doi:10.4028/www.scientific.net/KEM.813.191.

[16] Temmler A, Willenborg E, Wissenbach K. Design surfaces by laser remelting. Phys Procedia 2011;12:419–30. doi:10.1016/j.phpro.2011.03.053.

[17] Temmler A, Willenborg E, Wissenbach K. Design surfaces by laser remelting: Designoberfl??chen durch Laserumschmelzen. Materwiss Werksttech 2015;46:692–703. doi:10.1002/mawe.201500345.

[18] De Giorgi C, Furlan V, Demir AG, Tallarita E, Candiani G, Previtali B. Laser micropolishing of AISI 304 stainless steel surfaces for cleanability and bacteria removal capability. Appl Surf Sci 2017;406. doi:10.1016/j.apsusc.2017.02.083.

[19] Ma CP, Guan YC, Zhou W. Laser polishing of additive manufactured Ti alloys. Opt Lasers Eng 2017;93:171–7. doi:10.1016/j.optlaseng.2017.02.005.

[20] Bhaduri D, Penchev P, Batal A, Dimov S, Soo SL, Sten S, et al. Laser polishing of 3D printed mesoscale components. Appl Surf Sci 2017;405:29–46. doi:10.1016/j.apsusc.2017.01.211.

[21] Rombouts M, Maes G, Hendrix W, Delarbre E, Motmans F. Surface finish after laser metal deposition. Phys Procedia 2013;41:810–4. doi:10.1016/j.phpro.2013.03.152.

[22] Townsend A, Senin N, Blunt L, Leach RK, Taylor JS. Surface texture metrology for metal additive manufacturing: a review. Precis Eng 2016;46:34–47. doi:10.1016/j.precisioneng.2016.06.001.

[23] Senin N, Thompson A, Leach R. Feature-based characterisation of signature topography in laser powder bed fusion of metals. Meas Sci Technol 2018;29:aa9e19. doi:10.1088/1361-6501/aa9e19.

[24] ISO. ISO 3274 Geometrical Product Specifications (GPS) - Surface texture: Profile method - Nominal characteristics of contact (stylus) instruments. 1996.

[25] ISO. Geometrical product specification (GPS) - Surface texture : Profile method - Terms , definitions and surface texture parameters EN ISO 4287:1998. 2009.

[26] Kong H, Leach R, Thompson A, Senin N. (2017) A metrology horror story : the additive surface . In : ASPEN / ASPE 2017 Spring Topical Meeting on Manufacture and Metrology of Structured and Freeform Surfaces for Functional Applications , 14-17 March 2017 , 2017:14–7.
[27] Leach RK, Bourell D, Carmignato S, Donmez A, Senin N, Dewulf W. Geometrical metrology for metal additive manufacturing. CIRP Ann 2019;68:677–700. doi:10.1016/j.cirp.2019.05.004.
[28] Pagani L, Qi Q, Jiang X, Scott PJ. Towards a new definition of areal surface texture parameters on freeform surface. Meas J Int Meas Confed 2017;109:281–91. doi:10.1016/j.measurement.2017.05.028.
[29] Zanini F, Pagani L, Savio E, Carmignato S. Characterisation of additively manufactured metal surfaces by means of X-ray computed tomography and generalised surface texture parameters. CIRP Ann 2019;68:515–8. doi:10.1016/j.cirp.2019.04.074.
[30] Yasa E, Kruth J. Application of Laser Re-Melting on Selective Laser Melting Parts. Adv Prod Eng Manag 2011;6:259–70.
[31] Demir AG, Previtali B. Investigation of remelting and preheating in SLM of 18Ni300 maraging steel as corrective and preventive measures for porosity reduction. Int J Adv Manuf Technol 2017;93:1–13. doi:10.1007/s00170-017-0697-z.
[32] Dadbakhsh S, Hao L, Kong CY. Surface finish improvement of LMD samples using laser polishing. Virtual Phys Prototyp 2010;5:215–21. doi:10.1080/17452759.2010.528180.
[33] Rosa B, Mognol P, Hascoët JY. Modelling and optimization of laser polishing of additive laser manufacturing surfaces. Rapid Prototyp J 2016;22:956–64. doi:10.1108/RPJ-12-2014-0168.
[34] Koike R, Misawa T, Aoyama T, Kondo M. Controlling metal structure with remelting process in direct energy deposition of Inconel 625. CIRP Ann 2018;67:237–40. doi:10.1016/j.cirp.2018.04.061.
[35] Ramos-Grez JA, Bourell DL. Reducing surface roughness of metallic freeform-fabricated parts using non-tactile finishing methods. Int J Mater Prod Technol 2004;21:297–316. doi:10.1504/IJMPT.2004.004944.
[36] Mohajerani S, Bordatchev E V., Tutunea-Fatan OR. Recent Developments in Modeling of Laser Polishing of Metallic Materials. Lasers Manuf Mater Process 2018;5:395–429. doi:10.1007/s40516-018-0071-5.
[37] ISO. ISO 25178-2:2012 Geometrical Product Specifications (GPS) – Surface Texture: Areal Part 2: Terms, Definitions and Surface Texture Parameters. 2012.
[38] ISO. ISO 25178-3:2012 Geometrical product specifications (GPS) — Surface texture: Areal — Part 3: Specification operators. n.d.
[39] Hafiz AMK, Bordatchev E V., Tutunea-Fatan RO. Influence of overlap between the laser beam tracks on surface quality in laser polishing of AISI H13 tool steel. J Manuf Process 2012;14:425–34. doi:10.1016/j.jmapro.2012.09.004.
[40] Wieland M, Hänggi P, Hotz W, Textor M, Keller BA, Spencer ND. Wavelength-dependent measurement and evaluation of surface topographies: Application of a new concept of window roughness and surface transfer function. Wear 2000;237:231–52. doi:10.1016/S0043-1648(99)00347-6.
[41] Hafiz AMK, Bordatchev E V., Tutunea-Fatan RO. Influence of overlap between the laser beam tracks on surface quality in laser polishing of AISI H13 tool steel. J Manuf Process 2012;14:425–34. doi:10.1016/j.jmapro.2012.09.004.
[42] Dong WP, Stout KJ. Two-dimensional fast Fourier transform and power spectrum for surface roughness in three dimensions. Proc Inst Mech Eng Part B J Eng Manuf 1995;209:381–91. doi:10.1243/pime_proc_1995_209_097_02.
[43] De Chiffre L, Lonardo P, Trumpold H, Lucca DA, Goch G, Brown CA, et al. Quantitative characterization of surface texture. CIRP Ann - Manuf Technol 2000;49:635–42. doi:10.1016/S0007-8506(07)63458-1.
[44] Thompson A, Senin N, Maskery I, Körner L, Lawes S, Leach R. Internal surface measurement of metal powder bed fusion parts. Addit Manuf 2018;20:126–33. doi:10.1016/j.addma.2018.01.003.
[45] Kane VE. Process Capability Indices. J Qual Technol 1986;18:41–52. doi:10.1080/00224065.1986.11978984.
[46] Montgomery D. Design and Analysis of Experiments. 7th ed. 2009.